# Orbits in static magnetically and dyonically charged Einstein-Euler-Heisenberg black hole spacetimes

Daniela Magos[*]
*Departamento de Física, Universidad Autńoma Metropolitana–Iztapalapa, Apartado Postal 55-534, C.P. 09340, Ciudad de México, México*

Nora Bretón[†]
*Departamento de Física, Centro de Investigación y de Estudios Avanzados del I.P.N., Apartado Postal 14-740, C.P. 07360, Ciudad de México, Mexico*

Alfredo Macías[‡]
*Physics Departament, Universidad Autńoma Metropolitana–Iztapalapa, PO. Box 55-534, C.P. 09340, Ciudad de México, Mexico*

(Received 11 July 2023; accepted 18 August 2023; published 7 September 2023)

In the framework of the nonlinear Euler-Heisenberg electrodynamics coupled to general relativity, we consider static Einstein-Euler-Heisenberg magnetically and dyonically charged black hole spacetimes. These black holes are characterized, as usual, by mass $M$, magnetic charge $Q_m$, electric charge $Q$ and the Euler-Heisenberg nonlinear parameter. We find all possible equatorial trajectories for neutral and charged test particles. We analyze the light rings by using the Plebański pseudometric. The shape of the shadow of these black holes is presented, discussed, and compared with the one of the corresponding Reissner-Nordström linear cases.

DOI: 10.1103/PhysRevD.108.064014

## I. INTRODUCTION

In 1936 Euler and Heisenberg (EH) proposed a nonlinear electrodynamics (NLED) in the framework of the Dirac's theory of positrons [1,2]. The weak field version of this theory results to be the effective theory arising from quantum electrodynamics (QED) after one-loop of nonperturbative quantization. It accounts for quantum mechanical vacuum corrections to the Maxwell-Lorentz theory. In this theory, the vacuum is treated as a medium endowed with a kind of dielectric constant, its polarizability and magnetizability are depicted by clouds of virtual charges surrounding the real currents and charges. Schwinger reformulated this one-loop effective Lagrangian in the QED scheme [3]. The Euler-Heisenberg effect can be direct measured [4] and therefore, it is a valid physical effect [5].

The Einstein theory of gravity coupled to the class of nonlinear electrodynamics proposed by Plebański [6] admits regular black hole solutions, [7–11], i.e., black hole spacetimes whose curvature invariants are nonsingular, nevertheless, it is not clear if these solutions satisfy the condition of geodesic completeness. Therefore, there exist nowadays a great revival of interest on it.

Recently, Ruffini *et al.* [12] studied Einstein-Euler-Heisenberg (EEH) static black hole solutions endowed with electric, magnetic monopole, and dyonic charges, and they reduced the solutions to screened Reissner-Nordström (RN) ones. Moreover, the nonlinear effects act only in the screening of the electric charge generating virtual charges around the real charges and currents and affect the geometry only through the screened values of the real charges, i.e., these are QED corrections to the black hole horizon, entropy, total energy, and maximally extractable energy. Therefore Euler-Heisenberg is considered as a screened Maxwell [13–17].

Another viewpoint is the work of Yajima *et al.* [18], they obtained, numerically or analytically, electrically, magnetically, and dyonically charged static black hole solutions. They treated nonlinearity parameters as free parameters and study the effective Euler-Heisenberg Lagrangian as a low energy limit of the Born-Infeld theory. This standard way to consider nonlinear contribution of the Euler-Heisenberg electrodynamics adds a term $Q^4/r^6$ in the mass-energy function $f(r)$ of the Maxwell linear electrodynamics, as can be seen in Refs. [18–25]. This additional term modifies the geometrical structure and the thermodynamics of the Maxwell theory.

[*]dmagos@xanum.uam.mx
[†]nora@fis.cinvestav.mx
[‡]amac@xanum.uam.mx

 

Additionally, Bandos *et al.* [26] proposed, the so-called modified Maxwell (ModMax) electrodynamics, another approach to consider nonlinear corrections to the Maxwell theory, they developed nonlinear corrections to the Maxwell-Lorentz theory which preserve electromagnetic duality and conformal invariance.

It is well known that light in gravitational fields propagates along curved lines instead of straight lines, and when the gravitational field is strong, like the one of a black hole, an observer could see a dark central area (*shadow*) around the black hole position [27]. The development of the Event Horizon Telescope (EHT), allows the study of supermassive black holes by direct imaging, as it is the image of the black hole M87* [28] at the center of the galaxy M87, or more recently, the image of Sgr A*, the black hole at the center of the Milky Way [29]. Together with the gravitational wave detection by LIGO and Virgo [30], and very soon also by LISA, enhance the possibility for studying the different features of black holes.

In this work, we follow the Ruffini approach, and focus our study on the trajectories of neutral massive, massless, and charged test particles in the spacetimes of magnetically and dyonically charged static EEH black holes. Additionally, we study light rings, by means of the Plebański pseudometric, related to the geometrical metric and to the electromagnetic energy-momentum tensor, since in NLED light orbits are null geodesics of it. We present and discuss the shadow of these static black holes.

The outline of this paper is as follows: in Sec. II we briefly revisit the Einstein-Euler-Heisenberg theory. In Sec. III we display the solution for a magnetically charged EEH spacetime, we present the equatorial trajectories for massless, massive neutral and charged test particles. Moreover we study the light ring using the Plebański pseudometric and the shape of the shadow of the solution is obtained. In Sec. IV we address the EEH dyonic solution. We calculate the equatorial trajectories for massive and massless neutral test particles, then we analyze the geodesic equations for dyonically charged test particles. Moreover, we study the light ring and the shape of the shadow of this dyonic black hole, and in Sec. V we summarize the results.

## II. THE EINSTEIN-EULER-HEISENBERG THEORY

The action of the Einstein general relativity theory minimally coupled to a NLED [12] reads

$$S = \frac{1}{4\pi G}\int_{M^4} d^4x\sqrt{-g}\left[\frac{1}{4}R - \mathcal{L}(X,Y)\right], \tag{1}$$

where $G$ is the Newton's constant, which we will take $G = 1$, $g$ is the determinant of the metric tensor, $R$ is the Ricci scalar, and $\mathcal{L}(X,Y)$ is the Lagrangian of the NLED theory, which depends on the only two independent relativistic invariants constructed with the Faraday tensor for the Maxwell field in four dimensions, i.e., the scalar $X$ and the pseudoscalar $Y$, given by

$$X = \frac{1}{4}F_{\mu\nu}F^{\mu\nu} = \frac{1}{2}(\mathbf{B}^2 - \mathbf{E}^2),$$
$$Y = \frac{1}{4}F_{\mu\nu}{}^*F^{\mu\nu} = \mathbf{E}\cdot\mathbf{B}, \tag{2}$$

where $\mathbf{E}$ and $\mathbf{B}$ are the electric field and the magnetic field strength, respectively, while $F_{\mu\nu}$ is the Faraday electromagnetic tensor, and ${}^*F_{\mu\nu}$ its dual, defined by

$${}^*F_{\mu\nu} = \frac{1}{2}\sqrt{-g}\epsilon_{\mu\nu\sigma\rho}F^{\sigma\rho}, \qquad \epsilon_{0123} = -1,$$
$${}^*F^{\mu\nu} = \frac{1}{2}\frac{1}{\sqrt{-g}}\epsilon^{\mu\nu\sigma\rho}F_{\sigma\rho}, \qquad \epsilon^{0123} = 1, \tag{3}$$

$\epsilon_{\mu\nu\sigma\rho}$ is completely antisymmetric and satisfies $\epsilon_{\mu\nu\sigma\rho}\epsilon^{\mu\nu\sigma\rho} = -4!$.

For the case of the Euler-Heisenberg theory [1],

$$\mathcal{L}(X,Y) = -X + \frac{2\alpha^2}{45m^4}(4X^2 + 7Y^2), \tag{4}$$

with $m$ the electron mass and $\alpha$ the fine structure constant. The linear Maxwell electrodynamics is recovered when $\alpha = 0$, $\mathcal{L}(X) = -X$. The Einstein equations are obtained varying the action Eq. (1) with respect to the metric $g_{\mu\nu}$

$$R_{\mu\nu} - \frac{1}{2}Rg_{\mu\nu} = 8\pi T_{\mu\nu}, \tag{5}$$

where $R_{\mu\nu}$ is the Ricci curvature tensor, the energy-momentum tensor $T_{\mu\nu}$ is given by,

$$T_{\mu\nu} = \frac{1}{4\pi}[g_{\mu\nu}\mathcal{L} - (\mathcal{L}_X F_{\mu\sigma} + \mathcal{L}_Y {}^*F_{\mu\sigma})F_\nu{}^\sigma], \tag{6}$$

the subscript on $\mathcal{L}$ stands for derivative with respect to the corresponding invariant. The variation with respect to the electromagnetic four-potential $A_\mu$ yields the electromagnetic field equations,

$$\nabla_\mu(\mathcal{L}_X F^{\mu\nu} + \mathcal{L}_Y {}^*F^{\mu\nu}) = 0, \tag{7}$$

and the Jacobi identities read

$$\nabla_\mu({}^*F^{\mu\nu}) = 0. \tag{8}$$

It is useful to introduce a Legendre dual description of the NLED theory [6], by means of the introduction of the antisymmetric tensor $P_{\mu\nu}$ defined by

$$d\mathcal{L}(X,Y) = -\frac{1}{2}P^{\mu\nu}dF_{\mu\nu}, \tag{9}$$

where $L(X,Y)$ is the Lagrangian density for the Euler-Heisenberg nonlinear electrodynamics, Eq. (4). In general it reads

$$P^{\mu\nu} = 2\frac{\partial \mathcal{L}}{\partial F_{\mu\nu}} = -[\mathcal{L}_X F^{\mu\nu} + \mathcal{L}_Y {}^*F^{\mu\nu}], \tag{10}$$

then the field equation, Eq. (7), can be written as [31],

$$\nabla_\mu P^{\mu\nu} = 0. \tag{11}$$

Equation (10) are the constitutive relations between the electric field strength $\mathbf{D}$ and the magnetic field $\mathbf{H}$ with the electric field $\mathbf{E}$, and magnetic field strength $\mathbf{B}$. For the EH theory, the dual Plebański tensor $P_{\mu\nu}$ takes the form

$$P_{\mu\nu} = F_{\mu\nu} - \frac{4\alpha^2}{45m^4}(4XF_{\mu\nu} + 7Y {}^*F_{\mu\nu}), \tag{12}$$

and the invariants of the tensor $P_{\mu\nu}$ can be written as

$$s = -\frac{1}{4}P_{\mu\nu}P^{\mu\nu}, \qquad t = -\frac{1}{4}P_{\mu\nu}{}^*P^{\mu\nu}, \tag{13}$$

where ${}^*P^{\mu\nu} = \frac{1}{2}\sqrt{-g}\epsilon^{\mu\nu\sigma\rho}P_{\sigma\rho}$. The structural function $\mathcal{H}$, can be written as

$$\mathcal{H}(s,t) = -\frac{1}{2}P^{\mu\nu}F_{\mu\nu} - \mathcal{L}. \tag{14}$$

For the Euler-Heisenberg theory the structural function (up to terms of higher order in $\alpha$) reads

$$H(s,t) = s - \frac{2\alpha^2}{45m^4}(4s^2 + 7t^2). \tag{15}$$

The energy-momentum tensor, Eq. (6), written in the $P$ frame, reads [6,32]

$$T_{\mu\nu} = \mathcal{H}_s P_{\mu\alpha}P_\nu{}^\alpha + g_{\mu\nu}(2s\mathcal{H}_s + t\mathcal{H}_t - \mathcal{H}). \tag{16}$$

Notice that the Maxwell linear electrodynamics is recovered when $F_{\mu\nu} = P_{\mu\nu}$. In the particular case of Euler-Heisenberg nonlinear electrodynamics, Eq. (4), the energy-momentum tensor written in the $F$ frame is given by

$$\begin{aligned} T_{\mu\nu} = \frac{1}{4\pi}\Bigg[&\left(1 - \frac{16\alpha^2}{45m^4}X\right)F_\mu{}^\beta F_{\nu\beta} \\ &- \frac{28\alpha^2}{45m^4}Y\left(F_\mu{}^\beta {}^*F_{\nu\beta} + {}^*F_\mu{}^\beta F_{\nu\beta}\right) \\ &- g_{\mu\nu}\left(X - \frac{2\alpha^2}{45m^4}(4X^2 + 21Y^2)\right)\Bigg], \end{aligned} \tag{17}$$

which is suitable for the study of magnetic phenomena, since it allows us to obtain exact magnetic solutions, while the $P$ framework is useful for the treatment of electric effects. From Eq. (16) with the structural function, Eq. (15), the energy-momentum tensor in terms of the dual variables reads

$$\begin{aligned} T_{\mu\nu} = \frac{1}{4\pi}\Bigg[&\left(1 - \frac{16\alpha^2}{45m^4}s\right)P_\mu{}^\beta P_{\nu\beta} \\ &+ g_{\mu\nu}\left(s - \frac{2\alpha^2}{45m^4}(12s^2 + 7t^2)\right)\Bigg], \end{aligned} \tag{18}$$

To recover the original variables we use the constitutive or material equations that relate $F_{\mu\nu}$ with $P_{\mu\nu}$. These are,

$$F_{\mu\nu} = H_s P_{\mu\nu} + H_t {}^*P_{\mu\nu} = P_{\mu\nu} - \frac{16\alpha^2}{45m^4}\left[sP_{\mu\nu} + \frac{7}{4}t{}^*P_{\mu\nu}\right]. \tag{19}$$

## III. MAGNETICALLY CHARGED EEH BLACK HOLE

We consider the following static spherically symmetric black hole line element:

$$ds^2 = -f(r)dt^2 + \frac{1}{f(r)}dr^2 + r^2(d\theta^2 + \sin^2\theta d\varphi^2), \tag{20}$$

with signature $\{-,+,+,+\}$ and $f(r) = 1 - \frac{2m(r)}{r}$, where $m(r)$ is the mass-energy function to be determined from the field equations. We look for magnetically charged black hole solutions. For vanishing electric field, $\mathbf{E} = 0$, and non-zero magnetic field strength, $\mathbf{B} \neq 0$, the pseudo-invariant $Y$ vanishes, and the gauge 4-potential reads

$$A_\mu = [0,0,0,-Q_m\cos\theta], \tag{21}$$

where $Q_m$ is the black hole magnetic charge. Consequently the Faraday tensor $F_{\mu\nu}$ is given by

$$F_{\mu\nu} = Q_m \sin\theta(\delta^2_\mu\delta^3_\nu - \delta^3_\mu\delta^2_\nu). \tag{22}$$

It is important to mention that there are only two independent Einstein equations, the $tt$ and $rr$-components are linear dependent, as well as the $\theta\theta$ and $\phi\phi$-components. From the $tt$-component of the Einstein field equations we have that

$$m'(r) = \left(1 - \frac{4\alpha^2}{45m^4}\frac{Q_m^2}{r^4}\right)\frac{Q_m^2}{2r^2}, \tag{23}$$

whose integration leads to the expression for the mass-energy function $m(r)$, hence, $f(r)$ can be written as

$$f(r) = 1 - \frac{2M}{r} + \frac{Q_m^2}{r^2}\left(1 - \frac{\alpha}{225\pi}\frac{Q_m^2}{E_c^2 r^4}\right), \tag{24}$$

where $M$ is the black hole mass, we have introduced the critical electric field strength $E_c = \frac{m^2c^3}{e\hbar} \sim 10^{16}$ V/cm. For fields stronger than $E_c$ the creation of electron-positron pairs from vacuum occurs. Throughout this paper we will take $c = \hbar = 1$. Notice that the linear Reissner-Nordström solution is recovered when $\alpha = 0$. As it happens for the electrically charged case [12,13], the magnetic charge is also screened, due to the Euler-Heisenberg vacuum polarization effect:

$$\hat{Q}_m = Q_m\left(1 - \frac{\alpha}{225\pi}B_Q^2(r)\right)^{1/2}, \tag{25}$$

where $B_Q(r)$ reads,

$$B_Q(r) = \frac{Q_m}{r^2 E_c}. \tag{26}$$

The horizon radii $r_{H_\pm}$ are determined by the condition $f(r_h) = 0$ [33,34], which is equivalent to solve the equation

$$r^2 - 2Mr + Q_m^2\left(1 - \frac{\alpha}{225\pi}B_Q^2\right) = 0, \tag{27}$$

whose roots are given by

$$r_{H_\pm} = M \pm \sqrt{M^2 - Q_m^2\left(1 - \frac{\alpha}{225\pi}B_{Q_\pm}^2\right)}, \tag{28}$$

where $r_\pm$ are the radii of the outer and inner horizons respectively, and $B_{Q_\pm} = B_Q(r_{H_{RN_\pm}})$ is the critical magnetic field evaluated at the Reissner-Norström event horizons. The extreme case occurs when the inner and the outer horizons are equal, $r_{H_-} = r_{H_+} = r_{H_e}$. Since $B_{Q_{he}} = B_Q(r_{RN_{he}} = Q_m = M) = \frac{Q_m}{M^2 E_c}$ it implies that $r_{H_e}^2 = M^2 = Q_m^2(1 - \frac{\alpha}{225\pi}B_{Q_e}^2) = \hat{Q}_m^2$.

### A. Trajectories of neutral test particles

Now, we study the trajectories of test particles in the spacetime of the magnetically charged EEH black hole. Due to the spherical symmetry, without loss of generality, we restrict ourselves to the motion on the equatorial plane.

The motion of neutral test particles is described by the geodesic equation

$$\frac{d^2x^\nu}{d\tau^2} + \Gamma^\nu{}_{\sigma\rho}\frac{dx^\sigma}{d\tau}\frac{dx^\rho}{d\tau} = 0, \tag{29}$$

using the metric, Eq. (20), and the $f(r)$, Eq. (24), its components read

$$\ddot{t} = -\frac{f'(r)}{f(r)}\dot{r}\,\dot{t}, \quad \Rightarrow \quad f(r)\ddot{t} + f'(r)\dot{r}\,\dot{t} = 0 \tag{30}$$

$$\ddot{r} = -\frac{1}{2}f(r)f'(r)\dot{t}^2 + \frac{1}{2}\frac{f'(r)}{f(r)}\dot{r}^2 + rf(r)\dot{\phi}^2, \tag{31}$$

$$\ddot{\phi} = -2\frac{\dot{r}\,\dot{\phi}}{r}, \quad \Rightarrow \quad r^2\ddot{\phi} + 2r\dot{r}\,\dot{t} = 0, \tag{32}$$

the dot means derivative with respect to the affine parameter $\tau$ and $f'(r) = df(r)/dr$. The constants of motion, associated with the Killing vectors $\partial_t$ and $\partial_\phi$ can be obtained by the first integration of the $t$ and $\phi$ components of the geodesic equation, i.e.,

$$\frac{d}{d\tau}[f(r)\dot{t}] = 0, \quad \Rightarrow \quad \mathcal{E} = f(r)\dot{t}, \tag{33}$$

$$\frac{d}{d\tau}[r^2\dot{\phi}] = 0 \quad \Rightarrow \quad l = r^2\dot{\phi}, \tag{34}$$

where $\mathcal{E}$ is the energy per unit mass and $l$ is the angular momentum per unit mass, of the test particle. From the Lagrangian $L = g_{\mu\nu}\dot{x}^\mu\dot{x}^\nu$, we have

$$L = -f(r)\dot{t}^2 + \frac{\dot{r}^2}{f(r)} + r^2\dot{\phi}^2, \tag{35}$$

where $L$ can take the values $\{-1, 0, 1\}$, corresponding to timelike, null, and spacelike geodesics, respectively. Replacing Eqs. (33) and (34) into Eq. (35) we obtain the radial equation of motion

$$\dot{r}^2 + f(r)\left(\frac{l^2}{r^2} - L\right) = \mathcal{E}^2, \tag{36}$$

thus the effective potential $V_{\text{eff}}$ reads

$$V_{\text{eff}} = f(r)\left(\frac{l^2}{r^2} - L\right). \tag{37}$$

#### 1. Orbits of massive test particles

The radius of circular orbits $r_c$ is determined by the following conditions,

$$\frac{dV_{\text{eff}}}{dr}(r_c) = 0, \qquad \dot{r}(r_c) = 0, \tag{38}$$

which explicitly read,

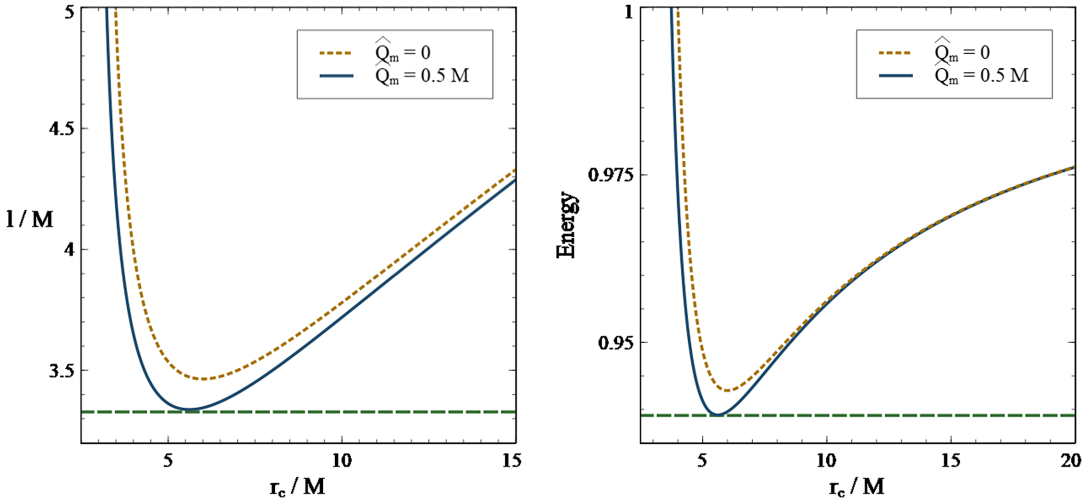


FIG. 1. We display the behavior of (left) the angular momentum $l/M$ and (right) the energy $\mathcal{E}$ of a circular orbit as a function of $r_c/M$, for fixed values of the mass $M = 10^5 M_\odot$ and $\hat{Q}_m = 0.5M$ (solid line), compared with the case $\hat{Q}_m = 0$ (dotted line). The dashed horizontal line indicates the minima of the functions $\mathcal{E}$ and $l$, $\mathcal{E}_{\min} \approx 0.9391$ and $l_{\min}/M = 3.328$.

$$r_c^3 - \frac{\hat{Q}_m^2 + l^2}{M} r_c^2 + 3l^2 r_c - 2\frac{l^2 \hat{Q}_m^2}{M} = 0, \tag{39}$$

$$(1-\mathcal{E}^2) r_c^4 - 2M r_c^3 + (l^2 + \hat{Q}_m^2) r_c^2 - 2M l^2 r_c + \hat{Q}_m^2 l^2 = 0, \tag{40}$$

where we have taken $L = -1$ since massive test particles travel on timelike geodesics. Equation (39) leads to

$$l^2 = \frac{r_c^2 (M r_c - \hat{Q}_m^2)}{r_c^2 - 3M r_c + 2\hat{Q}_m^2}, \tag{41}$$

replacing Eq. (41) into Eq. (40) leads to

$$\mathcal{E}^2 = \frac{(r_c^2 - 2M r_c + \hat{Q}_m^2)^2}{r_c^2 (r_c^2 - 3M r_c + 2\hat{Q}_m^2)}. \tag{42}$$

Figure 1 shows the behavior of the energy, Eq. (42), and the angular momentum, Eq. (41), as a function of the radius of the orbit. The solution of Eq. (39) provides us the radius of circular orbits for massive test particles, i.e.,

$$r_c = 2\sqrt{-\frac{p}{3}} \cos\left[\frac{1}{3}\arccos\left(\frac{3q}{2p}\sqrt{-\frac{3}{p}}\right) + \frac{2n\pi}{3}\right] + s, \tag{43}$$

the three roots correspond to $n = 0, 1, 2$, and $p$, $q$, and $s$ are given by

$$p = 3l^2 - \frac{1}{3}\left(\frac{\hat{Q}_m^2 + l^2}{M}\right), \tag{44}$$

$$q = \frac{l^2 (l^2 - \hat{Q}_m^2)}{M} - 2\left(\frac{l^2 + \hat{Q}_m^2}{3M}\right)^3, \tag{45}$$

$$s = \frac{l^2 + \hat{Q}_m^2}{3M}. \tag{46}$$

The root $n = 0$ corresponds to a minimum (stable circular orbit), while $n = 2$ to the maximum of the effective potential (unstable circular orbit). The root $n = 1$ is not physical, since it corresponds to a negative $r$. The radius of the innermost stable circular orbit (ISCO) $r_{is}$ is determined by the conditions for circular orbits, Eq. (38), plus

$$\frac{d^2 V_{\text{eff}}}{dr^2}(r_{is}) = 0, \tag{47}$$

which explicitly reads,

$$M r_{is}^3 - 6M^2 r_{is}^2 + 9M\hat{Q}_m^2 r_{is} - 4\hat{Q}_m^4 = 0, \tag{48}$$

whose solution is

$$r_{is} = 2M - \frac{3\hat{Q}_m^2 - 4M^2}{\sqrt[3]{\mathcal{B} + \sqrt{\mathcal{C}}}} + \sqrt[3]{\mathcal{B} + \sqrt{\mathcal{C}}}, \tag{49}$$

where we have introduced

$$\mathcal{B} = 8M^3 - 9M\hat{Q}_m^2 + \frac{2\hat{Q}_m^4}{M},$$
$$\mathcal{C} = 5M^2\hat{Q}_m^4 - 9\hat{Q}_m^6 + 4\frac{\hat{Q}_m^8}{M^2}. \tag{50}$$

It is worthwhile to mention that the radius of stable circular orbits, Eq. (43), with $n = 0$, for EEH is smaller than the one for the linear RN, while the radius of the ISCO, Eq. (49), is greater than the one for RN. In order to obtain the trajectories $r(\phi)$ of massive neutral particles, we use the

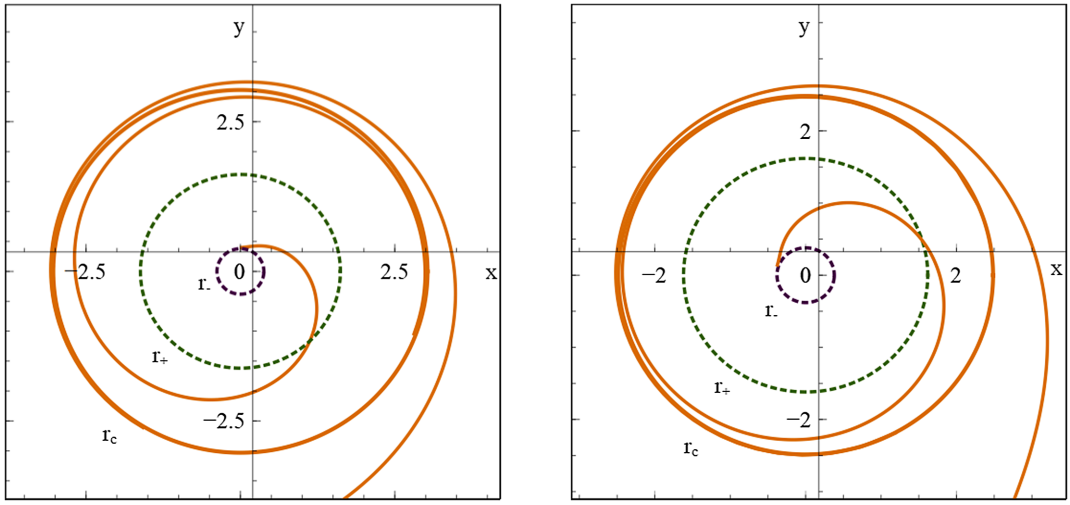


FIG. 2. The parametric plots $x = r\cos\phi(r)$, $y = r\sin\phi(r)$ are shown. The particle comes form infinity, it orbits some time at $r_c$, and then falls into the black hole. Massive neutral particles (left). Massless test particles (right). For fixed values of the mass $M = 10^4 M_\odot$, magnetic charge of the black hole $Q_m = 0.8M$ and angular momentum of the test particle $l = 4M$. $r_+$ and $r_-$ denote the outer and inner horizon radii respectively, and $r_c$ corresponds to the radius of the maximum of the effective potential, Eq. (37).

angular momentum written in terms of $\dot{\phi}$, Eq. (33), and the radial equation, Eq. (36), hence

$$\left(\frac{dr}{d\phi}\right)^2 = (\mathcal{E}^2 - V_{\text{eff}})\frac{r^4}{l^2}, \tag{51}$$

with the effective potential, Eq. (37). Performing the change of variable $u \equiv 1/r$, Eq. (51) reduces to

$$\Delta\phi = \int \Big[-Q_m^2 u^4 + 2Mu^3 - (1 + Q_m^2/l^2)u^2 + (\mathcal{E}^2 - 1 + 2Mu)/l^2\Big]^{-1/2} du. \tag{52}$$

Replacing the values of the angular momentum and the energy, Eqs. (41) and (42), into Eq. (52), we obtain that

$$\pm\phi = \int \left[-\hat{Q}_m^2 u^2 + 2(M - \hat{Q}_m^2 u_c)u + \left(M - \hat{Q}_m^2 u_c - \frac{M}{u_c^2 l^2}\right)u_c\right]^{-1/2} \frac{du}{u - u_c} + \text{constant}, \tag{53}$$

where $u_c = 1/r_c$ is the inverse of the radius, Eq. (43). It is useful to make the change of variable $\xi = \frac{1}{u-u_c}$, then

$$\pm\phi = \int \frac{d\xi}{\sqrt{c\xi^2 - b\xi - \hat{Q}_m^2}} + \text{constant}, \tag{54}$$

where

$$c = 3Mu_c - 4\hat{Q}_m^2 u_c^2 - \frac{M}{l^2 u_c}, \qquad b = 2(M - 2\hat{Q}_m^2 u_c). \tag{55}$$

Integrating Eq. (54) we obtain

$$\mp\phi = \begin{cases} \frac{1}{\sqrt{c}}\log\left(2\sqrt{c(-\hat{Q}_m^2 + b\xi + c\xi^2)} + 2c\xi + b\right), \\ -\frac{1}{\sqrt{-c}}\arcsin\left(\frac{2c\xi + b}{\sqrt{4\hat{Q}_m^2 c + b^2}}\right), \end{cases} \tag{56}$$

where the logarithmic function requires that $c > 0$ and the arcsin one that $c < 0$, the sign indicates the direction of the trajectory. The orbits for massive neutral test particles are shown in Fig. 2 (left).

### 2. Orbits of massless test particles

Since massless particles travel along null geodesics the effective potential is obtained taking $L = 0$ in Eq. (37), hence

$$V_{\text{eff}} = f(r)\left(\frac{l^2}{r^2}\right). \tag{57}$$

The circular orbits are determined by Eq. (38), which lead to

$$r_c^2 - 3Mr_c + 2\hat{Q}_m^2 = 0, \qquad r_c^4\mathcal{E}^2 - l^2(r_c^2 - 2Mr_c + \hat{Q}_m^2) = 0, \tag{58}$$

respectively. The solution to the quadratic equation reads

$$\Rightarrow \quad r_c = \frac{3}{2}M\left(1+\sqrt{1-\frac{8\hat{Q}_m^2}{9M^2}}\right), \tag{59}$$

$r_c$ corresponds to the maximum of the effective potential, it is the radius of an unstable circular orbit (UCO). Using the geodesic equations for $\phi$ and $r$, the trajectories $r(\phi)$ can be written as

$$\left(\frac{dr}{d\phi}\right)^2 = \left(\frac{\mathcal{E}^2}{l^2} - r^2 f(r)\right), \tag{60}$$

with $f(r)$, Eq. (24). Performing the change of variable $u = 1/r$, Eq. (60) becomes

$$\begin{aligned}\pm\phi &= \int \left[-\hat{Q}_m^2 u^4 + 2Mu^3 - u^2 + 1/\eta^2\right]^{-1/2} du, \\ &= \int [-\hat{Q}_m^2 u^2 + 2(M-\hat{Q}_m^2 u_c)u + (M-\hat{Q}_m^2 u_c)u_c]^{-1/2} \\ &\quad \times \frac{du}{u-u_c} + \text{constant}, \end{aligned} \tag{61}$$

where we have used the inverse of the impact parameter $\eta^2 \equiv \frac{\mathcal{E}^2}{l^2} = u_c^3(M-\hat{Q}_m^2 u_c)$, with $u_c$ obtained from the condition $V'_{\text{eff}}(u_c) = 0$, i.e.,

$$u_c = \frac{3M}{4\hat{Q}_m^2}\left(1-\sqrt{1-\frac{8\hat{Q}_m^2}{9M^2}}\right). \tag{62}$$

Performing the change of variable $\xi = \frac{1}{u-u_c}$, we obtain an equation like the one in Eq. (54), with

$$c = 3Mu_c - 4\hat{Q}_m^2 u_c^2, \qquad b = 2M - 4\hat{Q}_m^2 u_c. \tag{63}$$

whose solutions can be written as the ones in Eq. (56). The trajectories for massless test particles are shown in Fig. 2 (right), for fixed values of $M$, $Q_m$, and $l/M$. Notice that massless circular orbits are closer to the event horizon $r_+$ than the ones for massive test particles.

### B. Trajectories of charged test particles

The geodesic equations for a test particle with electric and magnetic charge $q_e$ and $q_m$, respectively, can be written as

$$\frac{d^2x^\nu}{d\tau^2} + \Gamma^\nu{}_{\sigma\rho}\frac{dx^\sigma}{d\tau}\frac{dx^\rho}{d\tau} = F^\nu_{\text{Lor}}, \tag{64}$$

where the right-hand side are the components of the Lorentz force $F^\nu_{\text{Lor}}$, which for the NLED theories can be written as follows, [35],

$$F^\nu_{\text{Lor}} = \left[-q_e F^\nu{}_\beta + q_m(-\mathcal{L}_X {}^*F^\nu{}_\beta + \mathcal{L}_Y F^\nu{}_\beta)\right]\dot{x}^\beta. \tag{65}$$

The function $\mathcal{L}$ is the Lagrangian of the NLED theory. For the Euler-Heisenberg case with $Y = 0$, the Lorentz force $F_{\text{Lor}}$ reduces to

$$F^\nu_{\text{Lor}} = \left[-q_e F^\nu{}_\beta + q_m\left(1-\frac{2\alpha}{45\pi}B_Q^2\right){}^*F^\nu{}_\beta\right]\frac{dx^\beta}{d\tau}, \tag{66}$$

and the geodesic equations read

$$\ddot{t} = -\frac{f'(r)}{f(r)}\dot{r}\,\dot{t} - \frac{q_m Q_m}{r^2 f(r)}\left(1-\frac{2\alpha}{45\pi}B_Q^2\right)\dot{r}, \tag{67}$$

$$\begin{aligned}\ddot{r} = &-\frac{1}{2}f(r)f'(r)\dot{t}^2 + \frac{1}{2}\frac{f'(r)}{f(r)}\dot{r}^2 + rf(r)\dot{\theta}^2 + rf(r)\sin^2\theta\dot{\phi}^2 \\ &- \frac{q_m Q_m f(r)}{r^2}\left(1-\frac{2\alpha}{45\pi}B_Q^2\right)\dot{t},\end{aligned} \tag{68}$$

$$\ddot{\theta} = -\frac{2}{r}\dot{r}\,\dot{\theta} + \sin\theta\cos\theta\dot{\phi}^2 + \frac{q_e Q_m \sin\theta}{r^2}\dot{\phi}, \tag{69}$$

$$\ddot{\phi} = -\frac{2}{r}\dot{r}\,\dot{\phi} - 2\cot\theta\dot{\theta}\,\dot{\phi} - \frac{q_e Q_m}{r^2\sin\theta}\dot{\theta}. \tag{70}$$

On the equatorial plane, Eq. (69) implies that

$$\frac{q_e Q_m}{r^2}\dot{\phi} = 0 \quad \Rightarrow \quad q_e = 0, \tag{71}$$

i.e., test particles with both charges cannot be on the equatorial orbits. The angular momentum is given in Eq. (34), while the energy $\mathcal{E}$ can be obtained by the first integration of Eq. (67), i.e.,

$$\frac{d}{d\tau}[f(r)\dot{t}] = \frac{q_m Q_m}{r^2}\left(1-\frac{2\alpha}{45\pi}B_Q^2\right)\frac{dr}{d\tau}, \tag{72}$$

$$\Rightarrow \quad \mathcal{E} = f(r)\dot{t} + \frac{\hat{q}_m\hat{Q}_m}{r}, \tag{73}$$

where $\hat{q}_m$ is the screened charge of the test particle, given by

$$\hat{q}_m = q_m\left(1-\frac{19\alpha}{225\pi}B_Q^2(r)\right)^{1/2}. \tag{74}$$

Replacing the conserved quantities $\mathcal{E}$ and $l$, Eqs. (34) and (73), into the line element, Eq. (20), with $\theta = \pi/2$, we obtain

$$\dot{r}^2 + f(r)\left(\frac{l^2}{r^2}+1\right) - \left(\mathcal{E} - \frac{\hat{q}_m\hat{Q}_m}{r}\right)^2 = 0, \tag{75}$$

this equation is of the form $\dot{r}^2 + V_{\text{eff}} = 0$, hence

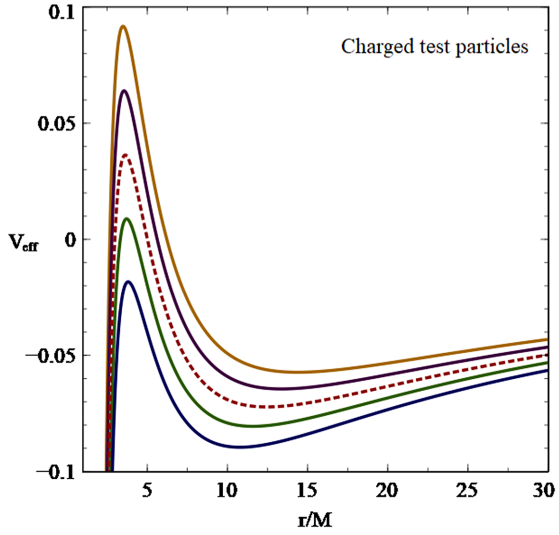


FIG. 3. Effective potential for a magnetically charged test particle. For fixed values of the mass $M = 10^4 M_\odot$ and the screened black hole charge $\hat{Q}_m = 0.8M$, the energy $\mathcal{E}/\mu = 1$, the angular momentum $l = 4M$ and increasing the charge of the test particle from bottom to top $\hat{q}_m/\mu = \{-0.2, -0.1, 0, 0.1, 0.2\}$. The dotted line corresponds to $\hat{q}_m = 0$.

$$V_{\text{eff}} = f(r)\left(\frac{l^2}{r^2} + 1\right) - \left(\mathcal{E} - \frac{\hat{q}_m \hat{Q}_m}{r}\right)^2. \tag{76}$$

The behavior of the effective potential depends on the product of the screened charges of the test particle $\hat{q}_m$ and of the black hole $\hat{Q}_m$, as it is shown in Fig. 3, it can also be seen that there exist a minimum and a maximum, indicating the existence of stable and unstable circular orbits. The conditions for the circular orbits are given by Eq. (38), with $V_{\text{eff}}$, Eq. (76), which lead to a third degree polynomial in $r_c$,

$$r_c^3 - \frac{\hat{Q}_m^2 + l^2 - \hat{q}_m^2 \hat{Q}_m^2}{M - \mathcal{E}\hat{q}_m \hat{Q}_m} r_c^2 + \frac{3l^2 M}{M - \mathcal{E}\hat{q}_m \hat{Q}_m} r_c - \frac{2l^2 \hat{Q}_m^2}{M - \mathcal{E}\hat{q}_m \hat{Q}_m} = 0, \tag{77}$$

whose solution is given in Eq. (43), with

$$p = \frac{9Ml^2(M - \mathcal{E}\hat{q}_m \hat{Q}_m) - (l^2 + \hat{Q}_m^2(1 - \hat{q}_m^2))^2}{3(M - \mathcal{E}\hat{q}_m \hat{Q}_m)^2}, \tag{78}$$

$$q = \frac{l^2[M(l^2 - \hat{Q}_m^2(1 + \hat{q}_m^2)) + 2\mathcal{E}\hat{q}_m \hat{Q}_m^3]}{(M - \mathcal{E}\hat{q}_m \hat{Q}_m)^2} - \frac{2[l^2 + \hat{Q}_m^2(1 - \hat{q}_m^2)]^3}{27(M - \mathcal{E}\hat{q}_m \hat{Q}_m)^3}, \tag{79}$$

$$s = \frac{l^2 + \hat{Q}_m^2(1 - \hat{q}_m^2)}{3(M - \mathcal{E}\hat{q}_m \hat{Q}_m)}. \tag{80}$$

Moreover, the radius of the ISCO, $r_{is}$, is obtained from Eq. (47), namely

$$r_{is}^3 - 6Mr_{is}^2 + \frac{3\hat{Q}_m^2(3M - 2\hat{q}_m \hat{Q}_m \mathcal{E} + \hat{q}_m^2 M)}{M - \hat{q}_m \hat{Q}_m \mathcal{E}} r_{is} - \frac{4\hat{Q}_m^2(\hat{Q}_m^2 - \hat{q}_m^2 \hat{Q}_m^2)}{M - \hat{q}_m \hat{Q}_m \mathcal{E}} = 0, \tag{81}$$

and the angular momentum for the ISCO, $l_{is}$, reads

$$l_{is}^2 = -\frac{2(\hat{q}_m \hat{Q}_m \mathcal{E} - M)r_{is}^3 + 3(\hat{Q}_m^2 - \hat{q}_m^2 \hat{Q}_m^2)r_{is}^2}{3r_{is}^2 - 12Mr_{is} + 10\hat{Q}_m^2}. \tag{82}$$

In order to find the trajectories $r(\phi)$ we use Eqs. (34) and (75) to obtain that

$$\left(\frac{dr}{d\phi}\right)^2 = -\left[f(r)\left(\frac{l^2}{r^2} + 1\right) - \left(\mathcal{E} - \frac{\hat{q}_m \hat{Q}_m}{r}\right)^2\right]\frac{r^4}{l^2}. \tag{83}$$

Using the solution for circular orbits, Eq. (43), and performing the change of variable $u = 1/r$, one obtains

$$\pm\phi = \int \left[-\hat{Q}_m^2 u^2 + 2(M - \hat{Q}_m^2 u_c)u + \left(M - \hat{Q}_m^2 u_c - \frac{M - \mathcal{E}\hat{q}_m \hat{Q}_m}{u_c^2 l^2}\right)u_c\right]^{-1/2} \frac{du}{u - u_c}, \tag{84}$$

where $u_c = 1/r_c$ with $r_c$ from Eq. (43) with Eqs. (78)–(80). It is useful to make the change of variable $\xi = \frac{1}{u - u_c}$, therefore Eq. (84) reduces to Eq. (54), whose solution is Eq. (56), with

$$c = 3Mu_c - 4\hat{Q}_m^2 u_c^2 - \frac{M - \mathcal{E}\hat{q}_m \hat{Q}_m}{l^2 u_c^2}, \qquad b = 2(M - 2\hat{Q}_m^2 u_c). \tag{85}$$

The circular orbits for a magnetically charged test particle are shown in Fig. 4. The orbits are very similar to the ones of neutral test particles in Fig. 2 (right), but the charged test particles fall into the black hole slower than the uncharged ones. It is interesting to note that the radius of stable circular orbits for massive and charged test particles on the EEH spacetime are smaller than the ones for RN. Moreover, for EEH black hole, the radius of unstable circular orbits for massive, charged, and massless test particles are greater than the ones for RN. Additionally, the ISCO radius for massive and charged particles of EEH, are greater than the ones for RN.

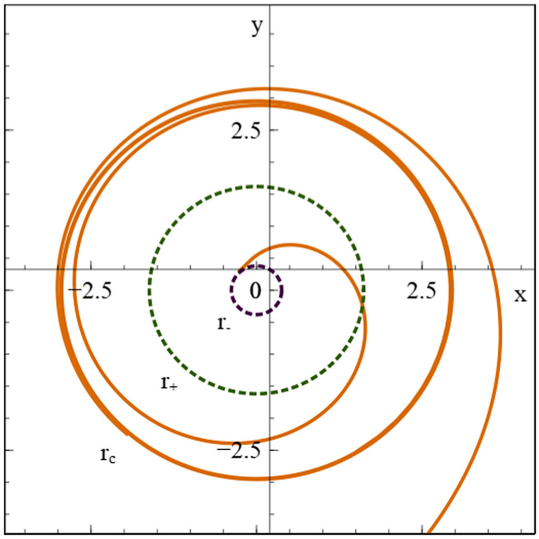


FIG. 4. The parametric plots $x = r\cos\phi(r)$, $y = r\sin\phi(r)$ for magnetically charged test particles. For fixed values of the mass $M = 10^4 M_\odot$ and magnetic black hole screened charge $\hat{Q}_m = 0.8M$, test particle angular momentum $l = 4M$, screened charge $\hat{q}_m = 0.1$ and energy $\mathcal{E} = 1$. $r_+$ and $r_-$ are the outer and inner horizon radii and $r_c$ is the radius of the circular orbit.

### C. Photons trajectories

In Maxwell-Lorentz linear electrodynamics, the discontinuities of the field propagate according to the equation for the characteristic surfaces, that in standard optics is known as eikonal equation. On a curved spacetime the equation for the characteristic surfaces is $g^{\mu\nu}S_{,\mu}S_{,\nu} = 0$, where $S_{,\mu}$ are the normal vectors to the characteristic surface $S$, the corresponding linear photons travel along null geodesics of the geometrical metric $g^{\mu\nu}$.

In nonlinear electrodynamics, photons propagate along null geodesics of the effective Plebański pseudometric $\gamma^{\mu\nu}$ [6,36], given by

$$\gamma^{\mu\nu} = g^{\mu\nu} + \frac{64\pi\alpha^2}{45m^4}T^{\mu\nu}, \tag{86}$$

which differs from the geometrical metric $g^{\mu\nu}$, since it contains the energy-momentum tensor $T^{\mu\nu}$ as well. For the EH nonlinear theory, with the energy-momentum tensor $T_{\mu\nu}$, Eq. (17), and $Y = 0$, up to the leading order in $\alpha$, it can be written as

$$\gamma^{\mu\nu} = \left(1 + \frac{16\alpha^2}{45m^4}X\right)g^{\mu\nu} + \frac{16\alpha^2}{45m^4}F^{\mu}{}_{\beta}F^{\nu\beta}. \tag{87}$$

The propagation equation for the nonlinear electromagnetic field discontinuities read $\gamma^{\mu\nu}S_{,\mu}S_{,\nu} = 0$. For the EEH theory the propagation equation reads

$$\left[\left(1 + \frac{16\alpha^2}{45m^4}X\right)g^{\mu\nu} + \frac{16\alpha^2}{45m^4}F^{\mu\beta}F^{\nu}{}_{\beta}\right]S_{,\mu}S_{,\nu} = 0. \tag{88}$$

Therefore, the energy-momentum tensor, $T_{\mu\nu}$, of the EH nonlinear field is responsible for the fact that these surfaces are not null surfaces of the geometrical metric. Nevertheless, for $\alpha = 0$, i.e., linear Maxwell-Lorentz electrodynamics, both metrics coincide. Then the trajectories for nonlinear photons are determined by

$$\gamma_{\mu\nu}\dot{x}^\mu\dot{x}^\nu = \left[\left(1 + \frac{16\alpha^2}{45m^4}X\right)g_{\mu\nu} + \frac{16\alpha^2}{45m^4}F_{\mu}{}^{\beta}F_{\nu\beta}\right]\dot{x}^\mu\dot{x}^\nu = 0. \tag{89}$$

On the equatorial plane, this equation reads,

$$f(r)\left(1 + \frac{2\alpha}{45\pi}B_Q^2\right)\dot{t}^2 - \frac{1}{f(r)}\left(1 + \frac{2\alpha}{45\pi}B_Q^2\right)\dot{r}^2 - r^2\left(1 - \frac{2\alpha}{45\pi}B_Q^2\right)\dot{\phi}^2 = 0. \tag{90}$$

The conserved quantities, energy $\mathcal{E}$, and angular momentum $l$ are given by

$$\mathcal{E} = \left(1 + \frac{2\alpha}{45\pi}B_Q^2\right)f(r)\dot{t}, \tag{91}$$

$$l = r^2\left(1 - \frac{2\alpha}{45\pi}B_Q^2\right)\dot{\phi}. \tag{92}$$

Then, from Eq. (90) one has that

$$\dot{r} = \left(1 - \frac{2\alpha}{45\pi}B_Q^2\right)\sqrt{R(r)}, \tag{93}$$

where we have introduced the effective potential

$$R(r) = \mathcal{E}^2\left[1 - \frac{f(r)}{r^2}\frac{l^2}{\mathcal{E}^2}\left(1 + \frac{2\alpha}{45\pi}B_Q^2\right)^2\right]. \tag{94}$$

Photons on the light ring satisfy the following conditions,

$$R'(r_{ph}) = 0, \qquad R(r_{ph}) = 0, \tag{95}$$

the first condition implies that $V_{\text{eff}'}(r_c) = 0$, with $V_{\text{eff}}(r)$ the effective potential for massless test particles, Eq. (57), i.e. $r_{ph} = r_c$, Eq. (59). From the second condition in Eq. (95) we can obtain the impact parameter $\eta$,

$$\eta^2 \equiv \frac{l^2}{\mathcal{E}^2} = \frac{r_c^2}{f(r_c)}\left(1 - \frac{2\alpha}{45\pi}B_Q^2\right)^2. \tag{96}$$

Then, up to the leading term in $\alpha$, the orbit equation reads

$$\pm\frac{\phi}{\left(1+\frac{2\alpha}{45\pi}B_Q^2\right)}=\int\frac{dr}{\frac{r^2}{l}\left(1-\frac{2\alpha}{45\pi}B_Q^2\right)\sqrt{R(r)}}=\int\frac{du}{[-\hat{Q}^2u^4+2Mu^3-u^2+1/\eta_B^2]^{1/2}},\tag{97}$$

where $\eta_B\equiv\eta/(1-\frac{2\alpha}{45\pi}B_Q^2)$ with $\eta$, Eq. (96). Notice that the integral has the same form of the deflection angle for massless particles, Eq. (61), thus, the solution is Eq. (54), with $c$ and $b$ given in Eq. (63). The EH contribution increases the deflection angle for nonlinear photons relative to the one for massless test particles, since from Eq. (97), $\phi_{ph}=(1+\frac{2\alpha}{45\pi}B_Q^2)\phi_{\text{Massless}}$. It is interesting to note that for EEH black hole, the radius of unstable circular orbits for photons are grater than the ones for RN.

### D. Shadow of the magnetically charged EEH black hole

As we already mentioned, the spacetime curvature deflects the light trajectories. In particular the strong gravitational fields, like the ones generated by black holes, are able to increase the deflection angles significantly. In particular, they can produce unstable circular orbits of light around them, the so called light rings. Since the orbits are not stable, part of the photons leaves them and gets out to a distant observer and the other part of them goes into the event horizon and falls down into the black hole interior.

From the equations of motion, we can write the four-momentum for a photon $P_\mu=\gamma_{\mu\nu}\dot{x}^\nu$

$$P_\mu=\left(-\mathcal{E},\frac{\sqrt{R(r)}}{f(r)},0,l\right).\tag{98}$$

For a distant observer located at fixed $r_0$, whose word lines are perpendicular to the plane $t_0$, we can choose a basis as follows

$$e^\mu_{(t)}=\left(\frac{1}{\sqrt{f(r)}},0,0,0\right),\qquad e^\mu_{(r)}=\left(0,\sqrt{f(r)},0,0\right),$$
$$e^\mu_{(\theta)}=\left(0,0,\frac{1}{r},0\right),\qquad e^\mu_{(\phi)}=\left(0,0,0,\frac{1}{r}\right).\tag{99}$$

Then, the four moment in this basis is $P^{(\alpha)}=\eta^{(\alpha\beta)}e^\mu_{(\beta)}P_\mu$

$$P^{(\alpha)}=\left(\frac{\mathcal{E}}{\sqrt{f(r)}},\sqrt{\frac{R(r)}{f(r)}},0,\frac{l}{r}\right).\tag{100}$$

Using the impact parameter, Eq. (96), we can write the celestial coordinates $(x,y)$ as follows

$$x=-r_0\left(\frac{P^{(\phi)}}{P^{(t)}}\right)\Big|_{r=r_0}=-\sqrt{f(r_0)}\eta,\tag{101}$$

$$y=r_0\left(\frac{P^{(\theta)}}{P^{(t)}}\right)\Big|_{r=r_0}=0.\tag{102}$$

These are the coordinates of the parametric equation of a circle whose radius is the radius of the shadow $r_{sh}$ of the black hole,

$$x^2+y^2=f(r_0)\eta^2=r_{sh}^2.\tag{103}$$

Replacing Eq. (96) into Eq. (103) we obtain

$$r_{sh}=r_c\left(1-\frac{2\alpha}{45\pi}B_Q^2(r_c)\right)\sqrt{\frac{f(r_0)}{f(r_c)}}.\tag{104}$$

The radius of the shadow of the RN black hole is $r_{sh}^{\text{RN}}=r_c\sqrt{\frac{f(r_0)}{f(r_c)}}$, therefore, the radius of the shadow for the EEH black hole is always smaller than the RN one, $r_{sh}^{\text{EEH}}<r_{sh}^{\text{RN}}$, as can be seen in Table I and Fig. 5. Figure 6 shows the radius of the shadow of magnetic EEH and RN black holes, for fixed values of the mass and magnetic charge, varying the position of the observer at $r_0$. As can be seen in Fig. 7, the radius of the black hole shadow $r_{sh}$ measured by an observer located at fixed $r_0$ with an angle $\beta$, can be approximated through elementary trigonometry, by

$$r_{sh}=r_0\sin\beta.\tag{105}$$

Using that $\cot\beta=\sqrt{\frac{\gamma_{11}}{\gamma_{33}}}\frac{dr}{d\phi}\Big|_{r=r_0}$ and some trigonometric identities, we find that for $r_0\to\infty$, $B_Q^2(r_0)=0$, and the radius of the black hole shadow coincides with Eq. (104).

TABLE I. The values of the radii of the shadow for magnetically charged EEH and RN are shown, for different values of the magnetic charge $Q_m$, as indicated in the table, for fixed mass $M=10^4M_\odot$. The Schwarzschild case is recovered when $Q_m=0$, and then $r_{sh}=5.19615$. $\hat{Q}_m$ is the screened magnetic charge.

| $Q_m$ | $\hat{Q}_m$ | $r_{sh}^{\text{RN}}(Q_m)$ | $r_{sh}^{\text{EEH}}(\hat{Q}_m)$ |
|---|---|---|---|
| 0.1 | 0.0999997 | 5.18748 | 5.18509 |
| 0.2 | 0.199998 | 5.16124 | 5.1515 |
| 0.3 | 0.299993 | 5.11683 | 5.09409 |
| 0.4 | 0.399982 | 5.0531 | 5.01046 |
| 0.5 | 0.499962 | 4.96827 | 4.89661 |
| 0.6 | 0.599928 | 4.85957 | 4.74591 |
| 0.7 | 0.699873 | 4.72274 | 4.5469 |
| 0.8 | 0.79978 | 4.55088 | 4.27775 |
| 0.9 | 0.899618 | 4.33202 | 3.88859 |
| 1.0 | 0.999312 | 4.04697 | 3.20653 |

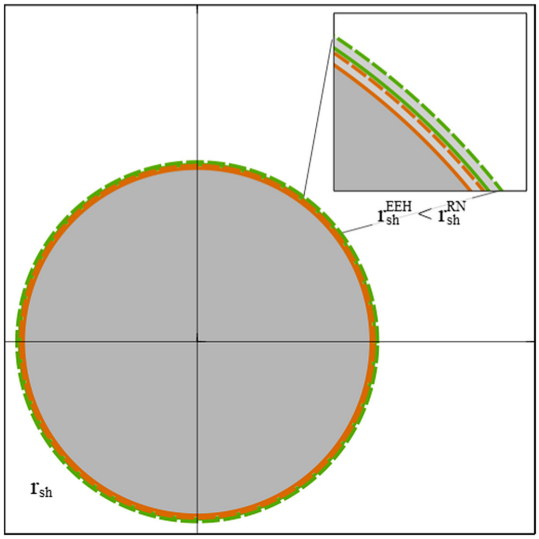


FIG. 5. The shadow of the magnetic EEH and RN black holes are shown. The continuous lines are for an observer at $r_0 = 50M$, and the dashed lines for a one at $r_0 \to \infty$. The fixed values are the mass $M = 10^4 M_\odot$, the magnetic charge $Q_m = 0.5M$, and the screened charge $\hat{Q}_m = 0.499962M$. On the corner, we display a zoom of the shadow, $r_{sh}^{EEH} < r_{sh}^{EEH}(r_0 \to \infty) < r_{sh}^{RN} < r_{sh}^{RN}(r_0 \to \infty)$.

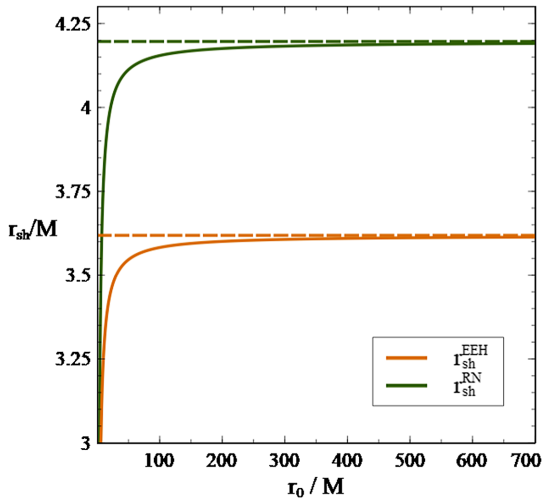


FIG. 6. The dashed lines correspond to the radius of the shadow for an observer placed at $r_0 \to \infty$, for EEH and RN black holes, respectively as indicated below the curves. The fixed values are the mass $M = 10^4 M_\odot$ and the magnetic charge $Q_m = 0.5M$, and the screened magnetic charge is $\hat{Q}_m = 0.499962M$. Notice that $r_{sh}^{EEH} < r_{sh}^{RN}$.

Observational constraints on magnetically charged EH-BH from the shadow are found in Vagnozzi *et al.* [20], derived from the EHT observations of the shadow of the central black hole in Sagittarius A*. According to [20], most of the effect on the shadow size comes from the magnetic charge rather than from the nonlinear EH parameter and $\mu \approx 0.3$ is the largest allowed coupling before the perturbative approach to the theory around the Maxwell Lagrangian ceases to be meaningful. Constraints depends on whether the charge regime is less or greater than 1, $Q_m < 1$ or $Q_m > 1$. For $Q_m < 1$ the upper limits are $Q_m \leq 0.7M(1\sigma)$ or $Q_m \leq 0.8M(2\sigma)$, for $\mu \approx 0.3$.

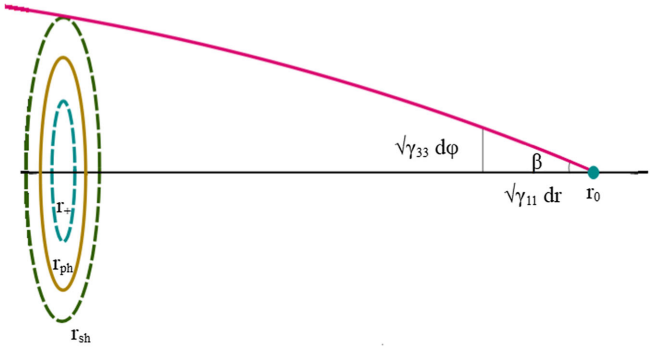


FIG. 7. The EEH black hole shadow measured by an observer at $r_0$. $r_+$ is the outer horizon radius, $r_{ph}$ is the light ring radius and $r_{sh}$ is the radius of the shadow.

For $Q_m > 1$ there appears a sharp discontinuity in the shadow radius due to the existence of a singularity in the nonlinear electromagnetic effective metric. The consistency with the EHT observations requires that $Q_m \approx 1.25M$ for $\mu \approx 0.3$; while for a lesser $\mu$ the consistency allows $1.1M \leq Q_m \leq 1.5M$.

## IV. DYONICALLY CHARGED EINSTEIN-EULER-HEISENBERG STATIC BLACK HOLE

Now, we consider a black hole endowed with electric and magnetic charges, $Q$ and $Q_m$, respectively, the electromagnetic gauge potential reads [37]

$$A_\mu = [A_t(r), 0, 0, -Q_m \cos\theta], \tag{106}$$

while the nonzero components of the Faraday tensor $F_{\mu\nu}$, are $F_{01} = -F_{10}$, for the electric field, and $F_{23} = -F_{32}$, for the magnetic field. The $t$-component of the vector potential $A_t$ takes the form

$$A_t(r) = \frac{Q}{r}\left(1 - \frac{2\alpha}{225\pi}E_Q^2 - \frac{\alpha}{45\pi}B_Q^2\right), \tag{107}$$

where $B_Q = \frac{Q_m}{r^2 E_c}$ is the magnetic field strength, and the electric field $E_Q = \frac{Q}{r^2 E_c}$, with $E_c \equiv \frac{m^2 c^3}{e\hbar}$. The electric and magnetic fields read

$$E(r) \approx \frac{Q}{r^2} - \frac{2\alpha}{45\pi}\frac{Q^3}{E_c^2 r^6} - \frac{\alpha}{9\pi}\frac{B(r)^2}{E_c^2}\frac{Q}{r^2}, \tag{108}$$

$$B(r) = \frac{Q_m}{r^2}. \tag{109}$$

Therefore, the nonzero components of the Faraday tensor are

$$F_{01} = \frac{Q}{r^2}\left(1 - \frac{2\alpha}{45\pi}E_Q^2 - \frac{\alpha}{9\pi}B_Q^2\right), \qquad F_{23} = Q_m \sin\theta. \tag{110}$$

In this case, both $X$ and $Y$ invariants are nonvanishing [12], they read

$$X = -\frac{Q^2}{2r^4}\left(1 - \frac{2\alpha}{45\pi}E_Q^2 - \frac{\alpha}{9\pi}B_Q^2\right)^2 + \frac{Q_m^2}{2r^4}, \tag{111}$$

$$Y = \frac{QQ_m}{r^4}\left(1 - \frac{2\alpha}{45\pi}E_Q^2 - \frac{\alpha}{9\pi}B_Q^2\right). \tag{112}$$

The $tt$-component of the Einstein field equations leads to

$$m'(r) = \frac{E_c^2 r^2}{2}\left(E_Q^2 + B_Q^2 - \frac{\alpha}{45\pi}E_Q^4 - \frac{\alpha}{45\pi}B_Q^4 - \frac{\alpha}{9\pi}B_Q^2 E_Q^2\right). \tag{113}$$

To first order in $\alpha$, the metric function $f(r)$ can be written as a screened dyonic RN-like solution [12],

$$f(r) = 1 - \frac{2M}{r} + \frac{\hat{Q}^2}{r^2} + \frac{\hat{Q}_m^2}{r^2}, \tag{114}$$

where the screened electric and magnetic charges of the black hole are given by

$$\hat{Q} = Q\left(1 - \frac{\alpha}{225\pi}E_Q^2 - \frac{\alpha}{90\pi}B_Q^2\right)^{1/2}, \tag{115}$$

$$\hat{Q}_m = Q_m\left(1 - \frac{\alpha}{225\pi}B_Q^2 - \frac{\alpha}{90\pi}E_Q^2\right)^{1/2}. \tag{116}$$

The horizon radii $r_{h_\pm}$ are determined from the condition $f(r_h) = 0$, which leads to

$$r_{h_\pm} = M \pm \left[M^2 - Q^2\left(1 - \frac{\alpha}{225\pi}E_{Q_\pm}^2 - \frac{\alpha}{90\pi}B_{Q_\pm}^2\right) - Q_m^2\left(1 - \frac{\alpha}{225\pi}B_{Q_\pm}^2 - \frac{\alpha}{90\pi}E_{Q_\pm}^2\right)\right]^{1/2}, \tag{117}$$

where $E_{Q_\pm} = E_Q(r_{h_\pm}^{\rm RN})$ and $B_{Q_\pm} = B_Q(r_{h_\pm}^{\rm RN})$, with $r_{h_\pm}^{\rm RN}$ the horizons radii for the RN solution.

The extreme case is obtained when $r_{h_+} = r_{h_-}$. In Tables II and III the values for the inner horizon radius $r_{h_-}$ and the outer horizon radius $r_{h_+}$ are shown for different values of the magnetic charge. Notice that the EEH inner horizon radius is smaller, while the outer horizon is greater than the RN ones.

TABLE II. Comparison between the inner horizon radius of the Einstein-Euler-Heisenberg, $r_{EEH_-}$, with the one of the Reissner-Nordström, $r_{RN_-}$, black holes, for fixed values of the mass $M = 10^6 M_\odot$ and electric charge $Q = 0.8M$. $\hat{Q}$ and $\hat{Q}_m$ are the screened electric and magnetic charges, respectively.

| $\hat{Q}/M$ | $Q_m/M$ | $\hat{Q}_m/M$ | $r_{RN_-}$ | $r_{EEH_-}$ |
|---|---|---|---|---|
| 0.79963 | 0 | 0 | 0.4 | 0.39950 |
| 0.79964 | 0.1 | 0.0998931 | 0.40839 | 0.40789 |
| 0.79969 | 0.2 | 0.19983 | 0.43431 | 0.43382 |
| 0.79976 | 0.3 | 0.299824 | 0.48038 | 0.47991 |
| 0.79983 | 0.4 | 0.399861 | 0.55278 | 0.55236 |
| 0.79990 | 0.5 | 0.499914 | 0.66833 | 0.66798 |

TABLE III. Comparison between the outer horizon radius of the Einstein-Euler-Heisenberg, $r_{EEH_+}$, with the one of the Reissner-Nordström, $r_{RN_+}$, black holes, for fixed values of the mass $M = 10^6 M_\odot$ and $Q = 0.8M$.

| $\hat{Q}/M$ | $Q_m/M$ | $\hat{Q}_m/M$ | $r_{RN_+}$ | $r_{EEH_+}$ |
|---|---|---|---|---|
| 0.7999985 | 0 | 0 | 1.6 | 1.60049 |
| 0.7999984 | 0.1 | 0.0999995 | 1.59161 | 1.59212 |
| 0.7999981 | 0.2 | 0.199999 | 1.56569 | 1.56618 |
| 0.7999997 | 0.3 | 0.299998 | 1.51962 | 1.52009 |
| 0.7999966 | 0.4 | 0.399997 | 1.44721 | 1.44763 |
| 0.7999940 | 0.5 | 0.499995 | 1.33166 | 1.33202 |

### A. Trajectories of neutral test particles

The motion of neutral test particles is described by the geodesic equations, Eq. (29). The conserved quantities are the energy $\mathcal{E}$ and the angular momentum $l$, Eq. (33), with the metric function $f(r)$ given in Eq. (114).

The effective potential has the same form as the one in Eq. (37), with $f(r)$, Eq. (114), which is displayed in Fig. 8 for massive timelike ($L = -1$) and massless null ($L = 0$) test particles, with two different values of the angular momentum $l$.

#### 1. Orbits of massive test particles

The equatorial circular motion for massive test particles is the same as the one for the magnetically charged black hole, replacing $\hat{Q}_m^2 \to \hat{Q}_m^2 + \hat{Q}^2$, the functions $\mathcal{B}$ and $\mathcal{C}$ for the ISCO radius, Eq. (49), are now given by

$$\mathcal{B} = 8M^3 + \frac{2(\hat{Q}^4 + \hat{Q}_m^4)}{M} - 9M(\hat{Q}^2 + \hat{Q}_m^2), \tag{118}$$

$$\mathcal{C} = \frac{5M^4(\hat{Q}^4 + \hat{Q}_m^4) - 9M^2(\hat{Q}^6 + \hat{Q}_m^6) + 4(\hat{Q}^8 + \hat{Q}_m^8)}{M} + \frac{8\hat{Q}^4\hat{Q}_m^4 + 45M^2\hat{Q}^2\hat{Q}_m^2(\hat{Q}^2 + \hat{Q}_m^2) - 54M^4\hat{Q}^2\hat{Q}_m^2}{M}. \tag{119}$$

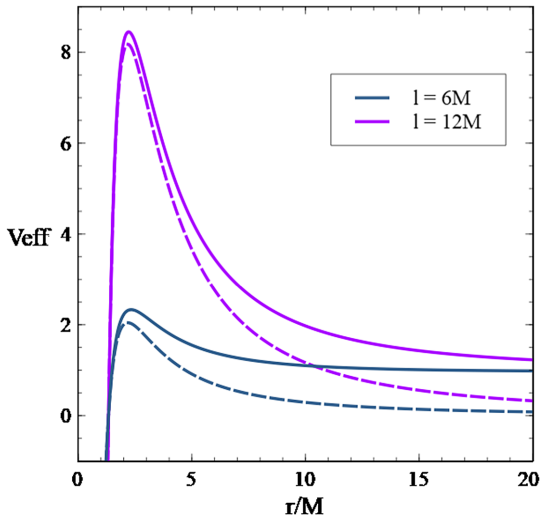


FIG. 8. The effective potential for massive (continuous line) and massless (dashed line) test particles are shown for angular momentum $l = 6M$ (bottom lines) and $l = 12M$ (upper lines). In both cases for fixed values of the mass $M = 10^5 M_\odot$, electric charge $Q = 0.5M$ and magnetic charge $Q_m = 0.8M$, ($\hat{Q} = 0.49829M$ and $\hat{Q}_m = 0.79813M$).

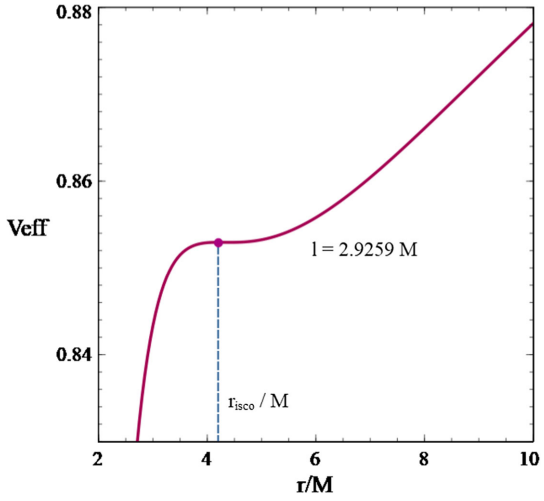


FIG. 9. The effective potential for the innermost stable circular orbit, for angular momentum of the test particle $l = 2.9259M$ and for fixed values of the mass $M = 10^5 M_\odot$, screened electric charge $\hat{Q} = 0.5M$ and screened magnetic charge $\hat{Q}_m = 0.8M$. The vertical line indicates the radius of the ISCO, $r_{is} \approx 4.1998M$.

Figure 9 shows the effective potential corresponding to the ISCO, for an angular momentum of the test particle $l = 2.9259M$. The deflection angle $\phi(r)$, for massive test particles is the same as the one in Eq. (54), with $c$ and $b$, Eq. (55), replacing $\hat{Q}_m^2 \to \hat{Q}_m^2 + \hat{Q}^2$. In Fig. 10 the orbits for massive neutral test particles are shown, $r_c$ corresponds to the maximum of the effective potential, Eq. (37), for $L = -1$, i.e., the radius of the unstable circular orbits. $r_{h_\pm}$ are the radii of the outer and inner horizons, given in Eq. (117).

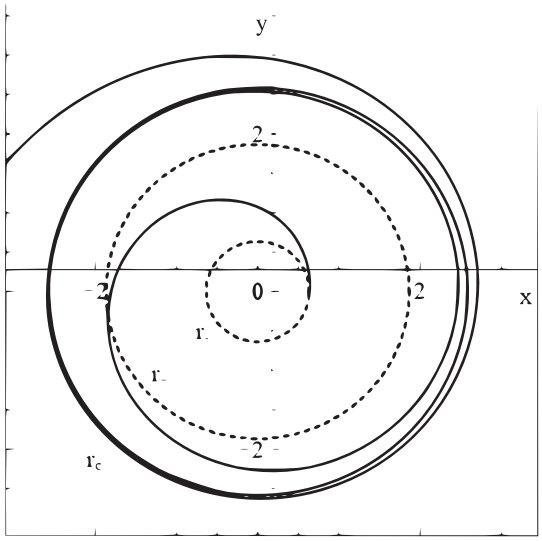


FIG. 10. The parametric plots $x = r\cos\phi(r)$, $y = r\sin\phi(r)$ for neutral test particles. For fixed values of the mass $M = 10^4 M_\odot$, screened electric and magnetic charges of the black hole $\hat{Q} = 0.5M$ and $\hat{Q}_m = 0.8M$, respectively, angular momentum $l = 4M$. $r_+$ and $r_-$ stand for the outer and inner horizon radii and $r_c$ is the stable circular orbit radius.

### 2. Orbits of massless test particles

The effective potential for massless test particles is given in Eq. (57) with $f(r)$, Eq. (114). In order to find the circular orbits, Eq. (38) must be satisfied, as before. The radius for the UCO is the same as Eq. (59) replacing once again $\hat{Q}_m^2 \to \hat{Q}_m^2 + \hat{Q}^2$. Similar to the massive case, the deflection angle has the form of Eq. (56), with the constants $c$ and $b$ given by Eq. (63), adding to the square of the magnetic charge the square of the electric charge of the black hole. The behavior of the circular orbits for massive and massless neutral test particles is very similar to the one shown in Fig. 2.

## B. Trajectories of dyonically charged test particles

The components of the geodesic equation, Eq. (64), with the Lorentz force, Eq. (65), read in this case

$$\ddot{t} = -\frac{f'(r)}{f(r)}\dot{r}\,\dot{t} - \frac{1}{r^2 f(r)}\left[q_e Q\left(1 - \frac{2\alpha}{45\pi}E_Q^2 - \frac{\alpha}{9\pi}B_Q^2\right) - q_m Q_m\left(1 - \frac{2\alpha}{45\pi}B_Q^2 - \frac{\alpha}{9\pi}E_Q^2\right)\right]\dot{r}, \tag{120}$$

$$\ddot{r} = -\frac{1}{2}f(r)f'(r)\dot{t}^2 + \frac{1}{2}\frac{f'(r)}{f(r)}\dot{r}^2 + rf(r)\dot{\phi}^2 - \frac{f(r)}{r^2}\left[q_e Q\left(1 - \frac{2\alpha}{45\pi}E_Q^2 - \frac{\alpha}{9\pi}B_Q^2\right) - q_m Q_m\left(1 - \frac{2\alpha}{45\pi}B_Q^2 - \frac{\alpha}{9\pi}E_Q^2\right)\right]\dot{t}, \tag{121}$$

$$0 = \frac{1}{r^2}\left[q_e Q_m + q_m Q\left(1 - \frac{2\alpha}{45\pi}E_Q^2 - \frac{\alpha}{9\pi}B_Q^2\right)^2\right]\dot{\phi},$$
$$\ddot{\phi} = -\frac{2}{r}\dot{r}\dot{\phi}. \tag{122}$$

From the first integration of the $t$ equation we can obtain the conserved energy per unit mass, $\mathcal{E}$, of the charged test particle.

$$\mathcal{E} = f(r)\dot{t} - \left(\hat{q}_e\hat{Q} - \hat{q}_m\hat{Q}_m\right)\frac{1}{r}, \tag{123}$$

where the screened electric and magnetic charges are given as follows

$$\hat{q}_e = q_e\left(1 - \frac{19\alpha}{225\pi}E_Q^2 - \frac{19\alpha}{90\pi}B_Q^2\right)^{1/2}, \tag{124}$$

$$\hat{q}_m = q_m\left(1 - \frac{19\alpha}{225\pi}B_Q^2 - \frac{19\alpha}{90\pi}E_Q^2\right)^{1/2}. \tag{125}$$

The angular momentum per unit mass is given by $l = r^2\dot{\phi}$. Replacing the conserved quantities into the radial equation, we obtain the effective potential $V_{\text{eff}}$,

$$V_{\text{eff}} = f(r)\left(\frac{l^2}{r^2} + 1\right) - \left(\mathcal{E} + \frac{\Delta_q}{r}\right)^2, \tag{126}$$

where $\Delta_q \equiv \hat{q}_e\hat{Q} - \hat{q}_m\hat{Q}_m$. The circular orbits are determined by the conditions in Eq. (38), that in this case reduce to

$$r_c^3 - \frac{l^2 + \hat{Q}_m^2 + \hat{Q}^2 - \Delta_q^2}{M + \mathcal{E}\Delta_q}r_c^2 + \frac{3l^2M}{M + \mathcal{E}\Delta_q}r_c - \frac{2l^2(\hat{Q}_m^2 + \hat{Q}^2)}{M + \mathcal{E}\Delta_q} = 0, \tag{127}$$

$$(r_c^2 - 2Mr_c + \hat{Q}_m^2 + \hat{Q}^2)\frac{(l^2 + r_c^2)}{(\mathcal{E}r_c + \Delta_q)^2} = r_c^2. \tag{128}$$

From Eq. (127) we can obtain the angular momentum of the test particle

$$l^2 = \frac{r_c^2[(M + \Delta_q\mathcal{E})r_c + \Delta_q^2 - \hat{Q}_m^2 - \hat{Q}^2]}{r_c^2 - 3Mr_c + 2\hat{Q}_m^2 + 2\hat{Q}^2}. \tag{129}$$

The solution to Eq. (127) is Eq. (43), with

$$p = \frac{3Ml^2}{M + \mathcal{E}\Delta_q} - \frac{1}{3}\left(\frac{\Delta_q^2 - l^2 - \hat{Q}_m^2 - \hat{Q}^2}{M + \mathcal{E}\Delta_q}\right)^2, \tag{130}$$

$$q = \frac{2}{27}\left(\frac{\Delta_q^2 - \hat{Q}^2 - \hat{Q}_m^2 - l^2}{M + \mathcal{E}\Delta_q}\right)^3 - \frac{Ml^2(\Delta_q^2 - \hat{Q}_m^2 - \hat{Q}^2 - l^2)}{(M + \mathcal{E}\Delta_q)^2} - \frac{2l^2(\hat{Q}_m^2 + \hat{Q}^2)}{M + \mathcal{E}\Delta_q}, \tag{131}$$

$$s = \frac{l^2 + \hat{Q}_m^2 + \hat{Q}^2 - \Delta_q^2}{3(M + \mathcal{E}\Delta_q)}. \tag{132}$$

The radius of the ISCO, $r_{is}$, is obtained from the extra condition, Eq. (47). The angular momentum corresponding to the ISCO can be written as

$$l_{is}^2 = \frac{2(\mathcal{E}\Delta_q + M)r_{is}^3 - 3(\hat{Q}_m^2 + \hat{Q}^2 - \Delta_q^2)r_{is}^2}{3r_{is}^2 - 12Mr_{is} + 10(\hat{Q}_m^2 + \hat{Q}^2)}. \tag{133}$$

In order to determine the orbits for dyonic test particles, we can use as before the geodesic equations for $\phi$ and $r$. $\phi(r)$. They are given by Eq. (56) with $\hat{Q}_m^2 + \hat{Q}^2$ and

$$c = 3Mu_c - 4(\hat{Q}_m^2 + \hat{Q}^2)u_c^2 - \frac{M + \mathcal{E}\Delta_q}{l^2u_c^2}, \tag{134}$$

$$b = 2[M - 2(\hat{Q}_m^2 + \hat{Q}^2)u_c]. \tag{135}$$

For a detailed analysis of the geodesic equations of charged particles in the linear dyonic RN spacetime, see [38].

### C. Photons trajectories

As already mentioned nonlinear photons propagate along null geodesics of the effective Plebański pseudometric. From Eqs. (87) and (89), photons trajectories are determined by the equation

$$0 = -f(r)\left(1 + \frac{2\alpha}{45\pi}B_Q^2 + \frac{2\alpha}{45\pi}E_Q^2\right)\dot{t}^2 + \frac{1}{f(r)}\left(1 + \frac{2\alpha}{45\pi}B_Q^2 + \frac{2\alpha}{45\pi}E_Q^2\right)\dot{r}^2 + r^2\left(1 - \frac{2\alpha}{45\pi}B_Q^2 - \frac{2\alpha}{45\pi}E_Q^2\right)\dot{\phi}^2. \tag{136}$$

The conserved quantities, the energy $\mathcal{E}$ and angular momentum $l$ read

$$\mathcal{E} = \left(1 + \frac{2\alpha}{45\pi}B_Q^2 + \frac{2\alpha}{45\pi}E_Q^2\right)f(r)\dot{t},$$
$$l = r^2\left(1 - \frac{2\alpha}{45\pi}B_Q^2 - \frac{2\alpha}{45\pi}E_Q^2\right)\dot{\phi}. \tag{137}$$

Then, replacing Eq. (137) into Eq. (136) we obtain the radial equation

$$\dot{r} = \left(1 - \frac{2\alpha}{45\pi}B_Q^2 - \frac{2\alpha}{45\pi}E_Q^2\right)\sqrt{R(r)}, \tag{138}$$

where the effective potential is given by

$$R(r) = \mathcal{E}^2 - f(r)\frac{l^2}{r^2}\left(1 + \frac{2\alpha}{45\pi}B_Q^2 + \frac{2\alpha}{45\pi}E_Q^2\right)^2. \tag{139}$$

The light ring is determined by the conditions, Eq. (95), the first condition implies that $V_{\text{eff}'}(r_c) = 0$, i.e. $r_{ph} \equiv r_c$, where $r_c$ correspond to the radius of the unstable circular orbit of massless test particles, Eq. (59), with $\hat{Q}_m^2 \to \hat{Q}_m^2 + \hat{Q}^2$. Moreover, from Eq. (137) we can obtain the impact parameter $\eta^2 \equiv \frac{l^2}{\mathcal{E}^2}$

$$\eta^2 \approx \frac{r_c^2}{f(r_c)}\left(1 - \frac{2\alpha}{45\pi}B_Q^2(r_c) - \frac{2\alpha}{45\pi}E_Q^2(r_c)\right)^2. \tag{140}$$

Therefore, the geodesic equation for nonlinear photons can be written as

$$\frac{dr}{d\phi} = \frac{\left(1 - \frac{2\alpha}{45\pi}B_Q^2 - \frac{2\alpha}{45\pi}E_Q^2\right)r^2}{\left(1 + \frac{2\alpha}{45\pi}B_Q^2 + \frac{2\alpha}{45\pi}E_Q^2\right)}\sqrt{\frac{R(r)}{l^2}}. \tag{141}$$

Performing the change of variable $\xi = \frac{1}{u - u_c}$ we have

$$\mp \frac{\phi}{\left(1 + \frac{2\alpha}{45\pi}B_Q^2 + \frac{2\alpha}{45\pi}E_Q^2\right)} \approx \int \frac{d\xi}{\sqrt{c\xi^2 - b\xi - (\hat{Q}^2 + \hat{Q}_m^2)}}, \tag{142}$$

the result of the integral is Eq. (56), with $c$ and $b$ given in Eq. (63), with $\hat{Q}^2 + \hat{Q}_m^2$.

The deflection angle $\phi(r)$ for the dyonically charged black hole is greater than the one for the pure magnetically charged case, because of the extra term on the denominator of the left-hand side of Eq. (142).

### D. Shadow of the dyonically charged EEH black hole

The four-momentum for a photon in a basis for a distant observer at fixed $r_0$, whose word lines are perpendicular to the plane $t_0$ has the same form as in Eq. (100). Using the celestial coordinates $(x, y)$, Eq. (102), and the impact parameter, Eq. (140), we obtain the parametric equation of a circle, $x^2 + y^2 = f(r_0)\eta^2$, whose radius corresponds to the radius of the shadow $r_{sh}$ of the dyonically charged black hole

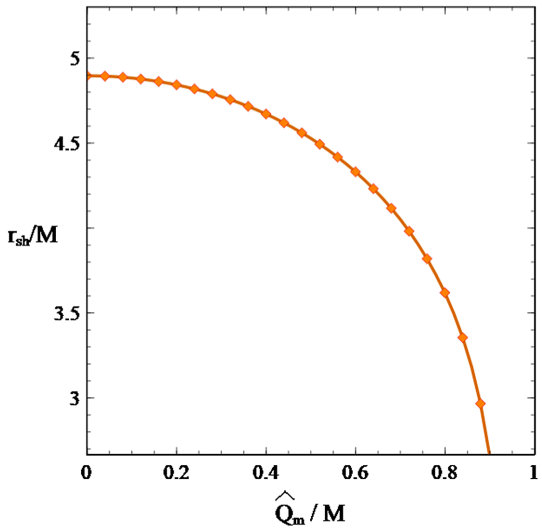


FIG. 11. The shadow radius for fixed values of the electric charge $Q = 0.5M$ and different values of the magnetic screened charge $\hat{Q}_m$, from 0 to $0.9M$ in 0.2 steps, with fixed mass $M = 10^4 M_\odot$.

$$r_{sh} = r_c\left(1 - \frac{2\alpha}{45\pi}B_Q^2(r_c) - \frac{2\alpha}{45\pi}E_Q^2(r_c)\right)\sqrt{\frac{f(r_0)}{f(r_c)}}. \tag{143}$$

The shadow radius for fixed value of the electric charge and different values of the magnetic screened charge is shown in Fig. 11. For the linear RN case, the shadow radius is $r_{sh}^{\text{RN}} = r_c\sqrt{\frac{f(r_0)}{f(r_c)}}$, the shadow of the EEH black holes is always smaller than the RN one, as can be seen in Table IV, Figs. 12 and 13.

TABLE IV. The values of the shadow radius for EEH and RN black holes are shown, for different values of the magnetic charge, for fixed values of mass $M = 10^4 M_\odot$ and electric charge $Q = 0.5M$.

| $Q_m$ | $\hat{Q}_m$ | $\hat{Q}$ | $r_{sh}^{\text{RN}}$ | $r_{sh}^{\text{EEH}}$ |
|---|---|---|---|---|
| 0 | 0 | 0.499962 | 4.96791 | 4.89605 |
| 0.1 | 0.0999806 | 0.499958 | 4.95824 | 4.88289 |
| 0.2 | 0.199958 | 0.499945 | 4.92891 | 4.84277 |
| 0.3 | 0.29993 | 0.499923 | 4.87902 | 4.77356 |
| 0.4 | 0.399891 | 0.499888 | 4.80687 | 4.67115 |
| 0.5 | 0.499836 | 0.499836 | 4.7096 | 4.52819 |
| 0.6 | 0.599753 | 0.499759 | 4.5825 | 4.33115 |
| 0.7 | 0.699621 | 0.499642 | 4.41723 | 4.05222 |
| 0.8 | 0.799397 | 0.499449 | 4.1966 | 3.6189 |
| 0.9 | 0.898935 | 0.499062 | 3.86892 | 2.66789 |

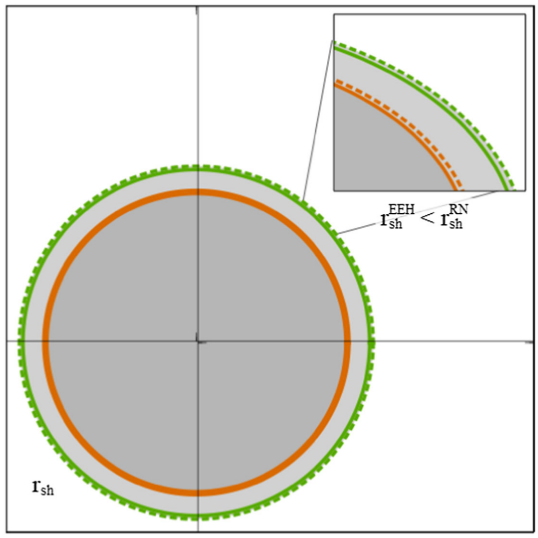


FIG. 12. The radii of the shadows of dyonic EEH and RN black holes are shown. The continuous lines corresponds to the shadow of EEH and RN black hole for an observer at $r_0 = 50M$, the dotted lines are the corresponding to an observer at $r_0 \to \infty$. The fixed values are the mass $M = 10^4 M_\odot$, the electric charge $Q = 0.8M$, and the magnetic charge $Q_m = 0.5M$. The square on the corner is a zoom to the shadow, notice that $r_{sh}^{EEH}(r_0) < r_{sh}^{EEH}(r_0 \to \infty) < r_{sh}^{RN}(r_0) < r_{sh}^{RN}(r_0 \to \infty)$.

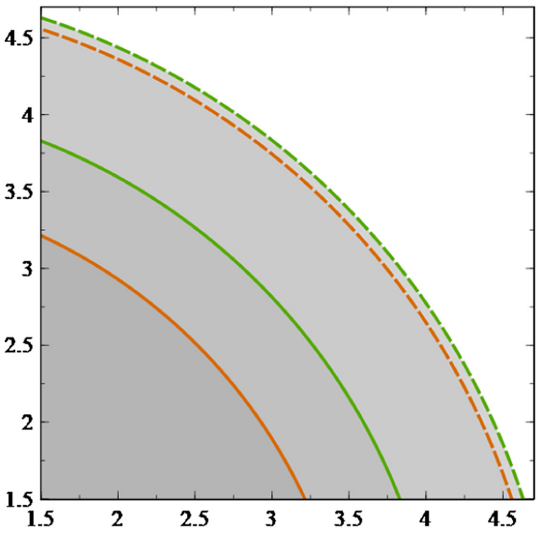


FIG. 13. The shadow radius for fixed values of the magnetic charge $Q_m = 0.5M$, black hole mass $M = 10^4 M_\odot$ and $r_0 = 50M$. From left to right: dyonic EEH and RN black holes shadows with electric charge $Q = 0.8M$, and the dashed lines are for magnetically charged EEH and RN black holes shadows.

## V. SUMMARY AND CONCLUSIONS

In this work, in the framework of the QED interpretation of the Euler-Heisenberg nonlinear electrodynamics, as a screening effect of the real charges, we studied the test particles orbits in magnetically and dyonically charged static Einstein-Euler-Heisenberg black hole spacetimes. These solutions represent a screened generalization of the linear magnetically and dyonically charged Reissner-Nordström black hole ones. For $\alpha = 0$ they reduce to the linear Reissner-Nordström solutions. If additionally, the charges are zero ($Q_m = Q = 0$), one recovers the Schwarzschild black hole. The screening effect on the charge extends a little the size of the RN event horizon, i.e., $r_+^{EEH} > r_+^{RN}$, while the inner horizon radius for EEH is smaller than the RN one, i.e., $r_-^{EEH} < r_-^{RN}$.

The study, of the equatorial motion of massive, massless, neutral, magnetically and dyonic charged test particles in these spacetimes, is performed by analyzing the effective potentials resulting from integration of the geodesic equations. The EH nonlinear contribution scantily modify stable and unstable circular trayectories of massive test particles. Moreover, the ISCO, almost imperceptibly stretches the one of RN case. We also calculated the orbits of charged test particles on the equatorial plane, resulting that for a magnetically charged black hole, only magnetically charged test particles can remain constrained, while for the dyonic black hole case, they can be endowed with both charges. It is important to note that in nonlinear electrodynamics, the Lorentz force is slightly different from the linear case, see Eq. (65)and [35]. It is worthwhile to note that the charges of the test particles are screened as well.

Moreover, the radius of stable circular orbits for both, massive and charged test particles in EEH blak hole spacetime, is smaller than the one of the RN black hole. While the radius of unstable circular orbits for massive, massless, and charged test particles as well as the ISCO for massive and charged particles in EEH, are a bit larger than the ones in RN. This is true for both the magnetic and dyonic black holes. Hence, the screening effect of the black hole charges on the orbits of neutral and charged test particles is hardly visible.

However, for the photons orbits the Euler-Heisenberg effect enhances, since, as already mentioned, nonlinear photons propagate on null geodesics, not of the geometrical metric $g_{\mu\nu}$, but of the effective Plebański pseudometric $\gamma_{\mu\nu}$ which contains additional to the geometric metric, the energy-momentum tensor $T_{\mu\nu}$ of the EH nonlinear electromagnetic field [6,39]. The effective potentials for the nonlinear photons remain always inside of that for the linear Reissner-Nordström ones. The deflection angle is larger than the one for massless test particles, for both the magnetic as well as the dyonic EEH black holes.

By using the effective Plebański pseudometric, we also calculate the shadow of the black holes, measured by a distant observer. We found that, due to the screening effect, Einstein-Euler-Heisenberg black hole shadows are always inside the shadows of the corresponding linear RN black holes, i.e., $r_{sh}^{EEH} < r_{sh}^{RN}$. Moreover, the radius of the shadow for the dyonic black hole is smaller than the shadow for the magnetic one, as can be seen in Fig. 13. In our study we

considered magnetic charges in the allowed ranges of the observational data of the shadow of Sagittarius A*; and as far as we know the actual precision in the shadow observations does not allow to rule out electromagnetically charged black holes.

It is worth mentioning that the tiny variations caused by the Euler-Heisenberg screening effect are almost negligible and hence very difficult to observe unless very precise measurements of the parameters of the black hole and the distance to the observer are obtained (cf. [13]), what is ordinarily not the case.

## ACKNOWLEDGMENTS

We especially thank Daniel Amaro for useful discussions and literature hints. D. M. has been sponsored by CONACyT-Mexico through the program *Estancias Posdoctorales por México*, modality 1.

[1] W. Heisenberg and H. Euler, Folgerungen aus der Diracschen theorie des positrons, Z. Phys. **98**, 714 (1936); English translation: Consequences of Dirac's theory of positrons, arXiv:physics/0605038.
[2] S. Weinberg, *The Quantum Theory of Fields* (Cambridge University Press, Cambridge, England, 1995).
[3] J. Schwinger, On gauge invariance and vacuum polarization, Phys. Rev. **82**, 664 (1951).
[4] G. Brodin, M. Marklund, and L. Stenflo, Proposal for Detection of QED Vacuum Nonlinearities in Maxwell's Equations by the Use of Waveguides, Phys. Rev. Lett. **87**, 171801 (2001).
[5] G. Boillat, Nonlinear electrodynamics: Lagrangians and equations of motion, J. Math. Phys. (N.Y.) **11**, 941 (1970).
[6] J. F. Plebański, *Lectures on Nonlinear Electrodynamics* (Nordita, Copenhagen, 1970).
[7] E. Ayón-Beato and A. García, Regular Black Hole in General Relativity Coupled to Nonlinear Electrodynamics, Phys. Rev. Lett. **80**, 5056 (1998).
[8] E. Ayón-Beato and A. García, New regular black hole solution from nonlinear electrodynamics, Phys. Lett. B **464**, 25 (1999).
[9] D. J. Cirilo Lombardo, Charge without charge, regular spherically symmetric solutions and the Einstein-Born-Infeld theory, Int. J. Theor. Phys. **48**, 2267 (2009).
[10] A. Burinskii and S. R. Hildebrandt, New type of regular black holes and particlelike solutions from nonlinear electrodynamics, Phys. Rev. D **65**, 104017 (2002).
[11] I. Dymnikova, Regular electrically charged vacuum structures with de Sitter centre in nonlinear electrodynamics coupled to general relativity, Classical Quantum Gravity **21**, 4417 (2004).
[12] R. Ruffini, Y.-B. Wu, and S.-S. Xue, Einstein-Euler-Heisenberg theory and charged black holes, Phys. Rev. D **88**, 085004 (2013).
[13] D. Amaro and A. Macías, Geodesic structure of the Euler-Heisenberg static black hole, Phys. Rev. D **102**, 104054 (2020).
[14] N. Bretón, C. Lämmerzahl, and A. Macías, Rotating structure of the Euler-Heisenberg black hole, Phys. Rev. D **105**, 104046 (2022).
[15] D. Amaro and A. Macías, Exact lens equation for the Einstein–Euler–Heisenberg static black hole, Phys. Rev. D **106**, 064010 (2022).
[16] N. Bretón, C. Lämmerzahl, and A. Macías, Type-D solutions of the Einstein-Euler-Heisenberg nonlinear electrodynamics with cosmological constant, Phys. Rev. D **107**, 064026 (2023).
[17] D. Amaro, C. Lämmerzahl, and A. Macías, Particle motion in the Einstein-Euler-Heisenberg rotating black hole spacetime, Phys. Rev. D **107**, 084040 (2023).
[18] H. Yajima and T. Tamaki, Black hole solutions in Euler-Heisenberg theory, Phys. Rev. D **63**, 064007 (2001).
[19] A. Allahyari, M. Allahyari, S. Vagnozzi, and D. F. Mota, Magnetically charged black holes from non-linear electrodynamics and the Event Horizon Telescope, J. Cosmol. Astropart. Phys. 02 (2020) 003.
[20] S. Vagnozzi, R. Roy, Y. D. Tsai, L. Visinelli *et al.*, Horizon-scale tests of gravity theories and fundamental physics from the Event Horizon Telescope image of Sagittarius A*, Classical Quantum Gravity **40**, 165007 (2023).
[21] D. Magos and N. Bretón, Thermodynamics of the Euler-Heisenberg-AdS black hole, Phys. Rev. D **102**, 084011 (2020).
[22] T. Karakasis, G. Koutsoumbas, A. Machattou, and E. Papantonopoulos, Magnetically charged Euler-Heisenberg black holes with scalar hair, Phys. Rev. D **106**, 104006 (2022).
[23] M. Maceda and A. Macías, Non-commutative inspired black holes in Euler-Heisenberg non-linear electrodynamics Phys. Lett. B **788**, 446 (2019).
[24] H. Rehman, G. Abbas, Tao Zhu, and G. Mustafa, Matter accretion onto the magnetically charged Euler-Heisenberg black hole with scalar hair, arXiv:2307.16155.
[25] N. Bretón and L. A. López, Birefringence and quasinormal modes of the Einstein-Euler-Heisenberg black hole, Phys. Rev. D **104**, 024064 (2021).
[26] I. Bandos, K. Lechner, D. Sorokin, and P. K. Townsend, A non-linear duality-invariant conformal extension of Maxwell's equations, Phys. Rev. D **102**, 121703 (2020).
[27] A. Grenzebach, *The Shadow of Black Holes, An Analytic Description* (Springer, Switzerland, 2016).
[28] The Event Horizon Telescope Collaboration, First M87 Event Horizon Telescope results. I. The shadow of the supermassive black hole, Astrophys. J. Lett. **875**, L1 (2019).
[29] The Event Horizon Telescope Collaboration, First Sagittarius A* Event Horizon Telescope results. I. The shadow of the supermassive black hole in the center of the Milky Way, Astrophys. J. Lett. **930**, L12 (2022).

[30] B. P. Abbott *et al.*, Observation of Gravitational Waves from a Binary Black Hole Merger, Phys. Rev. Lett. **116**, 061102 (2016).

[31] H. Salazar, A. Garcia D., and J. Plebański, Duality rotations and type D solutions to Einstein equations with nonlinear electromagnetic sources, J. Math. Phys. (N.Y.) **28**, 2171 (1987).

[32] G. W. Gibbons and C. A. R. Herdeiro, The Melvin universe in Born-Infeld theory and other theories of non-linear electrodynamics, Classical Quantum Gravity **18**, 1677 (2001).

[33] V. P. Frolov and I. D. Novikov, *Black Hole Physics* (Kluwer Academic Publisher, Netherlands, 1997).

[34] C. W. Misner, K. S. Thorne, and J. A. Wheeler, *Gravitation* (W.H. Freeman and Company, San Francisco, 1973).

[35] N. Bretón and C. E. Ramírez-Codiz, On the NUT-Born-Infeld-Λ spacetime, Ann. Phys. (Amsterdam) **353**, 252 (2015).

[36] S. A. Gutierrez, A. L. Dudley, and J. F. Plebański, Signals and discontinuities in general relativistic nonlinear electrodynamics, J. Math. Phys. (N.Y.) **22**, 2835 (1981).

[37] S. W. Hawking and S. F. Ross, Duality between electric and magnetic black holes, Phys. Rev. D **52**, 5865 (1995).

[38] S. Grunau and V. Kagramanova, Geodesics of electrically and magnetically charged test particles in the Reissner-Nordström space-time: Analytical solutions, Phys. Rev. D **83**, 044009 (2011).

[39] M. Novello, V. De Lorenci, J. Salim, and R. Klippert, Geometrical aspects of light propagation in nonlinear electrodynamics, Phys. Rev. D **61**, 045001 (2000).